A Multigrid InSAR Technique for Joint Analyses at Single-Look and Multi-Look Scales

Francesco Falabella, *Graduate Student Member, IEEE*, Carmine Serio, Guido Masiello, Qing Zhao, and Antonio Pepe, *Senior Member, IEEE*

***Abstract*— This work proposes a multigrid differential synthetic aperture radar (SAR) interferometry (InSAR) technique for the detection of ground displacements at different spatial scales. The method relies on efficient phase-unwrapping (PhU) operations performed at the native spatial scales. In particular, a set of multi-look interferograms are first unwrapped using conventional (or advanced) PhU algorithms at the regional scale. Subsequently, ML unwrapped interferograms are used to facilitate the PhU operations performed at the local scale (single-look). Specifically, the unwrapped multi-look interferograms are resampled to the single-look grid and modulo-2π subtracted to the single-look interferograms. These phase residuals are then unwrapped and added back to the multi-look resampled interferograms. To accomplish these operations, at variance with alternative multiscale methods, no (linear/nonlinear) models are used to fit the spatial high-pass phase residuals. Finally, the unwrapped single-look interferograms are properly inverted to retrieve the ground displacement time series using any small baseline (SB)-oriented multitemporal InSAR tool. Experimental results are performed by processing a set of SAR data acquired by the X-band COSMO-SkyMed sensor over the coastal area of Shanghai, China.**

***Index Terms*— Ground deformations, multigrid phase unwrapping (PhU), synthetic aperture radar interferometry (InSAR).**

I. Introduction

THE exploitation of synthetic aperture radar (SAR) images [1] through techniques as SAR interferometry (InSAR) represents a common practice nowadays to measure the topography and deformations of Earth's surface. In this context, differential InSAR techniques provide accurate measurements, with millimeter accuracy, of the ground deformations along the radar line-of-sight (LOS) direction. The multitemporal InSAR (Mt-InSAR) approaches, such as the persistent scatterer interferometry (PSI) [2] and the small baseline subset (SBAS) techniques [3], are helpful tools for remotely detecting, mapping, and monitoring surface deformation phenomena, due to their capability to produce spatially dense velocity maps and long-term displacement time series corresponding to coherent targets location. The pioneering SBAS technique was specifically designed to detect the distributed scatterers' (DSs) ground displacements. On the other hand, the PSI approaches focused on studying ground deformations of pointwise and coherent permanent scatterers (PSs) over the imaged scenes. In recent years, some Mt-InSAR techniques have also been proposed for investigating the deformation signals of both DS and PS targets [4], [5], which allow performing a complete analysis of the investigated scenes over medium-to-high coherent regions.

It is well known that the decorrelation phenomena [6] play a significant role in generating reliable ground displacement time series. These phenomena substantially impact the echoes' response returned from the targets to the sensor, and the consequence is an increased level of noise in the generated interferograms. A low signal-to-noise ratio (SNR) critically impacts analyzing the interferometric signals (i.e., inaccurate displacement time-series) using canonical interferometric SAR approaches. Principally, low SNR values negatively influence the accuracy of the phase-unwrapping (PhU) operation [1], which is the procedure to recover the full phase from the measured interferometric phases, whose values are restricted to the $[-\pi, +\pi)$ range. Since PhU is an ill-posed problem, there is no unique solution, and many PhU algorithms have been developed to handle this critical operation (see [7]–[11]).

The study of the ground deformations related to PS targets can be performed through several efficient Mt-InSAR techniques, which differ from the pioneering PSI approach [2], such as the adaptations of the SBAS algorithm [11]–[13] at the single-look (SL) spatial scale. These methods have revealed effective and robust; however, when applied in critical scenarios with considerable temporal decorrelation disturbances, the regional [multi-look (ML)] analyses are not accurate enough and degrade the products' quality at the local scale (single-look). This degradation is mostly attributable to a low density of stable investigated targets. As a matter of fact, the methodologies [11]–[13] and other alternative methods available in the

Manuscript received March 5, 2021; revised May 15, 2021; accepted May 31, 2021. Date of publication June 16, 2021; date of current version December 23, 2021. This work was supported in part by the Project OT4CLIMA through the Italian Ministry of Education, University and Research (D.D. 2261 of 6.9.2018, PON R&I 2014–2020 and FSC), and in part by the Dragon 5 European Space Agency (ESA) Project entitled "Global Climate Change, Sea Level Rise, Extreme Events and Local Ground Subsidence Effects in Coastal and River Delta Regions through Novel and Integrated Remote Sensing Approaches (GREENISH)" under Grant 58351. *(Corresponding author: Francesco Falabella.)*

Francesco Falabella is with the School of Engineering, University of Basilicata, 85100 Potenza, Italy, also with the Institute for the Electromagnetic Sensing of the Environment (IREA), National Research Council (CNR) of Italy, 80124 Naples, Italy, and also with the Institute of Methodologies for Environmental Analysis (IMAA), National Research Council (CNR) of Italy, 85050 Tito, Italy (e-mail: francesco.falabella@unibas.it).

Carmine Serio and Guido Masiello are with the School of Engineering, University of Basilicata, 85100 Potenza, Italy (e-mail: carmine.serio@unibas.it; guido.masiello@unibas.it).

Qing Zhao is with the Key Laboratory of Geographical Information Science, Ministry of Education, East China Normal University, Shanghai 200062, China, and also with the Joint Laboratory for Environmental Remote Sensing and Data Assimilation, East China Normal University, Shanghai 200062, China (e-mail: qzhao@geo.ecnu.edu.cn).

Antonio Pepe is with the Institute for the Electromagnetic Sensing of the Environment (IREA), National Research Council (CNR) of Italy, 80124 Naples, Italy (e-mail: pepe.a@irea.cnr.it).

Digital Object Identifier 10.1109/LGRS.2021.3086271

literature analyze the interferograms at the SL scale, benefiting from a dense network of DS pixels identified at the regional scale.

This letter proposes a novel multigrid hybrid technique that investigates stable targets' deformations at SL scale implementing a multigrid PhU procedure that, at variance with [11], [12], could limit the PhU errors propagation. The developed technique exploits the unwrapped phases at the regional scale to perform (local) PhU operations at the finer SL scale, which are performed by solving an L_1-norm problem [9], [10]. At variance with [11], [12], the proposed methodology's distinctive characteristic is that the unwrapped phases at the regional scale are exclusively used to facilitate the PhU of the SL interferograms. No least-square (LS) inversion procedures (between the regional and local scale) are applied before the PhU operations are performed at the SL scale, by circumventing the PhU errors' propagation due to the LS inversion and limiting other drawbacks of alternative Mt-InSAR solutions.

The proposed technique has been tested in the low-coherent coastal zone of the Shanghai megacity. The investigated area has long been subjected to severe ocean-reclamation projects to satisfy the growing land demand for industrial and urban development. Therefore, the selected case-study area is severely decorrelated [14]. The InSAR analyses are thus more challenging using canonical approaches so that our hybrid approach gives better results in this context. A set of 46 COSMO-SkyMed (CSK) SAR images acquired from 2013 to 2016, provided by the Italian Space Agency (ASI), have been used to test the proposed methodology.

II. Permanent and Distributed Scatterers Selection

The proposed technique first requires identifying the location of stable targets (both PSs and DSs). This operation is crucial because maximizing the spatial density of reliable and well-processed SAR pixels at both local and regional scales has mutual effects at both scales. To perform effectively PhU procedures, a suitable selection of the "stable" pixels is performed on the coarse (regional) and fine (local) resolution scales independently.

Given a set of N SAR images, two sets of M differential SAR interferograms at the regional $\varphi_i^{(\mathrm{ML})}$ $i = 1, 2, \ldots, M$ and local $\varphi_i^{(\mathrm{SL})}$ $i = 1, 2, \ldots, M$ spatial scales are preliminarily generated (see [3], [12]).

Due to the different statistical properties of the PSs and DSs [1], evaluating the stability of the two different classes of scatterers (PS and DS) has been carried out with distinctive strategies.

For what attain the coarser resolution, we select the stable DSs by analyzing the ML InSAR phases and their temporal relations over the entire set of available InSAR data pairs, as shortly outlined in [15]. In particular, from the generated multi-look interferograms, the following factor is computed:

$$\gamma_{\mathrm{DS}}(P) = \frac{1}{\Lambda}\left|\sum_{i=1}^{\Lambda} \exp\left[j\varphi_{\mathrm{Triang},i}^{(\mathrm{ML})}(P)\right]\right| \in [0, 1] \qquad (1)$$

where $j = \sqrt{-1}$ is the imaginary unit and $\varphi_{\mathrm{Triang},i}^{(\mathrm{ML})}(P) = \langle \varphi_{A,B}^{(\mathrm{ML})}(P) + \varphi_{B,C}^{(\mathrm{ML})}(P) + \varphi_{C,A}^{(\mathrm{ML})}(P)\rangle_{-\pi,+\pi}$ is the wrapped sum of three generic temporal connected ML InSAR phases (e.g., the i-th triplet), namely, $\varphi_{A,B}^{(\mathrm{ML})}(P)$, $\varphi_{B,C}^{(\mathrm{ML})}(P)$, and $\varphi_{C,A}^{(\mathrm{ML})}(P)$, which are computed by exploiting SAR images acquired at three time instants, namely, t_A, t_B, and t_C [15]. Note that P is a generic pixel of the investigated scene at the ML scale, Λ is the number of triplets that can be computed considering the generated ML interferograms and $\langle\cdot\rangle_{-\pi,+\pi}$ stands for the operator that wraps up the phase in the $[-\pi, +\pi)$ interval. The relation (1), also called triangular coherence, represents an equivalent estimator of DS targets' coherence [15]. Pixels with triangular coherence values greater or equal to a certain threshold $\gamma_{\mathrm{DS}}^{\mathrm{Threshold}}$, $S_{\mathrm{DS}} = \{P : \gamma_{\mathrm{DS}}(P) \geq \gamma_{\mathrm{DS}}^{\mathrm{Threshold}}\}$, are then considered coherent DS points. Over them, the subsequent operations at the regional scale are performed. Other strategies for selecting the DS coherent targets are also feasible, such as using the spatial coherence [1] or methods based on exploiting the statistical similarities of the scatterers involved in the ML resolution cells [5].

Differently, the PS targets location identification on the finest grid is made out using a spectral diversity estimator [11]. With this method, the PSs phase dispersion is evaluated by analyzing the difference between the two nonspectral-overlapped range looks as follows:

$$\gamma_{\mathrm{PS}}(P) = \frac{1}{M}\left|\sum_{i=1}^{M} \exp\left\{j\left[\varphi_i^{\mathrm{UP}}(P) - \varphi_i^{\mathrm{LOW}}(P)\right]\right\}\right| \in [0, 1] \quad (2)$$

where $\varphi_i^{\mathrm{UP}}(P)$ and $\varphi_i^{\mathrm{LOW}}(P)$, respectively, are the upper and lower spectra component of the checked SL pixel P. Similar to (1), we select the stable PS targets by imposing a threshold $\gamma_{\mathrm{PS}}^{\mathrm{Threshold}}$ such that the group of stable, PSs, obeys $S_{\mathrm{PS}} = \{P : \gamma_{\mathrm{PS}}(P) \geq \gamma_{\mathrm{PS}}^{\mathrm{Threshold}}\}$. Instead of (2), other methodologies can also be successfully applied for the identification of the stable PSs, e.g., amplitude dispersion-based estimator [2] or methods based on the exploitation of both amplitude and phase values [4], [5].

The groups of the individuated stable PSs and coherent DSs, namely, S_{PS} and S_{DS}, are those pixels over which the subsequent PhU operations at the SL and ML scales are performed, respectively.

III. Multigrid Algorithm

In this section, the focus is on the operations performed to get the interferometric unwrapped phase signals at the SL spatial scale by showing how the proposed methodology avoids some of the bottlenecks that arise in specific Mt-InSAR methods that work at SL scale [11]–[13].

We can split the proposed approach into two distinctive processing steps.

1) The first PhU operations are performed on the group of coherent DS pixels S_{DS}.
2) The final PhU step is directly applied at the SL scale on the group of stable PS targets S_{PS}, by considering the unwrapped phase values computed at the ML scale as a proxy to facilitate/improve PhU operations at the SL scale.

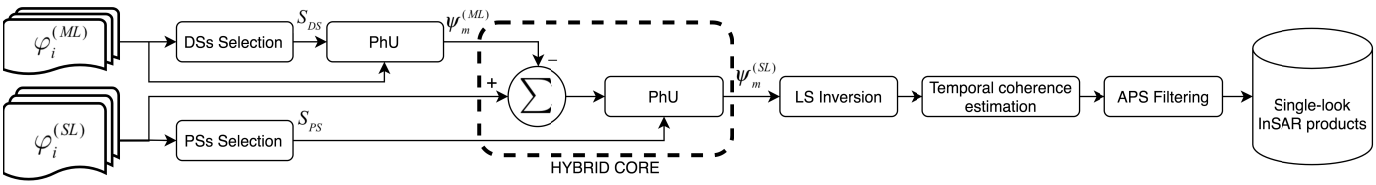

Fig. 1. Flow diagram of the developed hybrid multiscale InSAR approach.

We underline that the ML PhU operations can be set up with any L_1-solver currently available in the literature, such as the algorithms [9], [10] or using 3-D PhU tools.

We now focus on the core of the methodology. In this context, we follow a strategy that permits us to unwrap the SL InSAR phases related to the group of stable PS targets S_{PS} by circumventing some of the problems connected to PhU errors propagation through the interferograms' network [12], [13] or the aliasing phenomena [11].

The unwrapped phases at the SL scale $\psi_i^{(\mathrm{SL})}$ $i = 1, 2, \ldots, M$ are computed at the generic radar pixel P of the finer grid as follows:

$$\psi_m^{(\mathrm{SL})}(P) = \psi_m^{(\mathrm{ML})}(P) + \left\langle \varphi_m^{(\mathrm{SL})}(P) - \psi_m^{(\mathrm{ML})}(P) \right\rangle_{-\pi,+\pi} + 2\pi K_m(P), \quad m = 1, 2, \ldots, M \tag{3}$$

where $\psi_m^{(\mathrm{SL})}(P)$ and $\varphi_m^{(\mathrm{SL})}(P)$ are the unwrapped and wrapped SL phases, respectively, $\psi_m^{(\mathrm{ML})}(P)$ is the unwrapped ML phase computed at the coarser spatial grid and resampled over the finer grid, and $K_m(P)$ is the ambiguity number estimated during the PhU operation of the residual phase term $\langle \varphi_m^{(\mathrm{SL})} - \psi_m^{(\mathrm{ML})} \rangle_{-\pi,+\pi}$. In (3), the resampled ML unwrapped phases act as a model to help (and improve) the PhU operation at the SL scale. We want to stress that, differently from the method in [12], which requires the generation of the ground displacement time series at the regional scale (used to flatten the SL interferograms), our approach performs PhU operations directly at the SL scale on the (undistorted) set of differential residual interferograms $\langle \varphi_m^{(\mathrm{SL})} - \psi_m^{(\mathrm{ML})} \rangle_{-\pi,+\pi}$. PhU operations at the SL scale can be set using the same L_1-solver used for the PhU operations at the ML scale. Moreover, to increase the number of detectable SAR pixels at the SL scale, PhU operations can be complemented with region-growing local PhU procedures (see [13] and the references therein). In this way, also intermittent coherent SAR pixels at the SL scale might be finally analyzed.

We want to remark that, conversely, the method in [12] and other alternative Mt-InSAR multiscale [13], [16], [17] approaches rely on the analysis of the phase residuals $\langle \varphi_m^{(\mathrm{SL})} - \psi_m'^{(\mathrm{ML})} \rangle_{-\pi,+\pi}$, where $\psi_m'^{(\mathrm{ML})}$ are the resampled interferograms reconstructed from the ground displacement time series computed after the LS inversion of the ML interferograms. However, the LS inversion of the ML interferograms, which leads to the generation of the ground displacement time series, spreads the PhU mistakes all over the whole network of differential SAR interferograms, see also [18], affecting also those "reconstructed" interferograms that were originally well-unwrapped. Accordingly, the residual phases $\langle \varphi_m^{(\mathrm{SL})} - \psi_m'^{(\mathrm{ML})} \rangle_{-\pi,+\pi}$ might be erroneous because contaminated by time-uncorrelated PhU errors. This finding is critical, especially in low-coherent regions, and justifies the work presented in this letter. It is worth noting that, conversely, in medium-to-high coherent regions, the approaches in [11]–[13] result very robust. Finally, the LOS-projected ground displacement time series, containing the whole contributions due to the ground terrain movements and the differential displacements of the buildings/infrastructures and human-made objects, are directly obtained through the LS inversion (or a weighted LS inversion as proposed in [19]) of the SL unwrapped interferograms, see (3).

To check the reliability of the computed local ground displacement time series, we calculate the values of the temporal coherence [10], [11], [15], [18] factor that gives us feedback on the amount of time-uncorrelated PhU errors committed at the given SAR pixel. Reasonable values of the temporal coherence threshold $\gamma_{\mathrm{TEMP}}^{\mathrm{Threshold}}$ used to identify the well-processed SAR pixels at the SL scale lie in the $[0.6, 0.9]$ range. As a final step, the atmospheric phase screen (APS) is estimated and compensated from the obtained LOS-projected displacement time series [2], [3].

The working flow of the proposed hybrid multiscale InSAR approach is shown in Fig. 1.

IV. Experimental Results

The developed multiscale InSAR method has been tested on a set of SAR data acquired over the ocean-reclaimed lands of Lingang New City, Shanghai, China. The selected area is characterized by a mixture of new human-made structures and bare soil lands, subject to essential consolidation movements, especially in the slice of land next to the sea [14]. We used 46 VV polarized CSK (X-band) SAR images, spanning the time interval between December 2013 and January 2016, from which 104 differential SAR interferograms have been generated at both regional and local scales. The interferograms have been identified by imposing a maximum threshold on both orthogonal and temporal baseline values to reduce the decorrelation phenomena [6]. Expressly, we have set 250 days and 300 m for the orthogonal and temporal baseline thresholds, respectively. The two sets of SL and ML interferograms, with an ML factor of ten pixels for both the range and azimuth directions, were finally generated. We show in Fig. 2 the comparison of the SL flattened phase residuals related to two selected interferograms, computed with the strategy adopted in [12], [16], and [17], namely $\langle \varphi_m^{(\mathrm{SL})} - \psi_m'^{(\mathrm{ML})} \rangle_{-\pi,+\pi}$ (left side), and those analyzed with our method, namely $\langle \varphi_m^{(\mathrm{SL})} - \psi_m^{(\mathrm{ML})} \rangle_{-\pi,+\pi}$ (right side). The spurious phase signals that appear in Fig. 2(a) and (c) are the results of the time-uncorrelated PhU errors [18] that the SBAS LS inversion spreads all over the network of small baseline (SB) interfero-

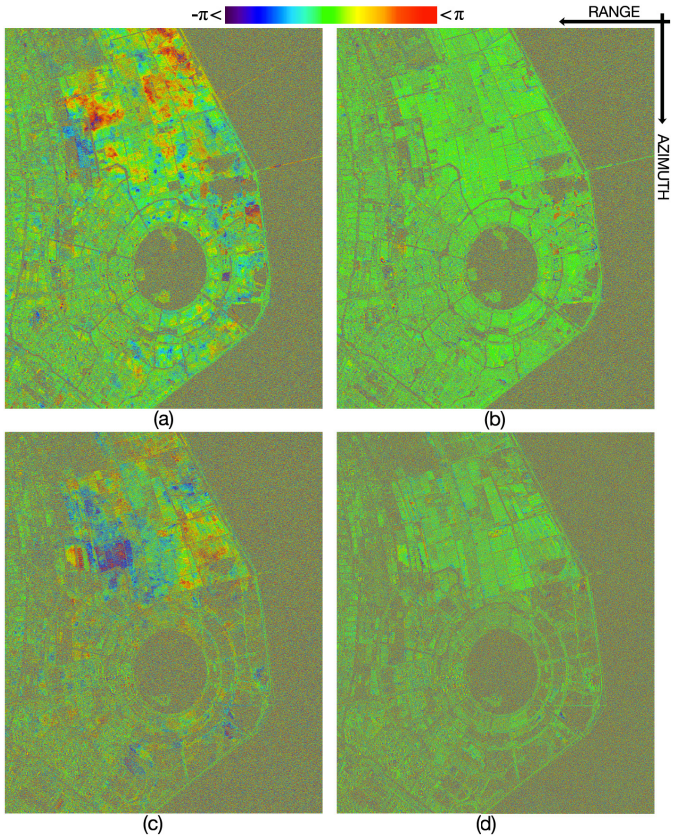

Fig. 2. Comparison of four selected full resolution residual SAR interferograms, focused on Lingang New City district, (a) and (c) are flatted by using the ground displacement time-series, strategy adopted in [12], [16], [17], whereas (b) and (d) are flatted by using the (undistorted) resampled ML unwrapped phases, as proposed in our multiscale technique. (a) and (b) Flattened interferograms calculated from the InSAR pair of the epochs January 19, 2015, and January 27, 2015. (c) and (d) Flattened interferograms calculated from the InSAR pair of the epochs January 24, 2014, and February 9, 2014.

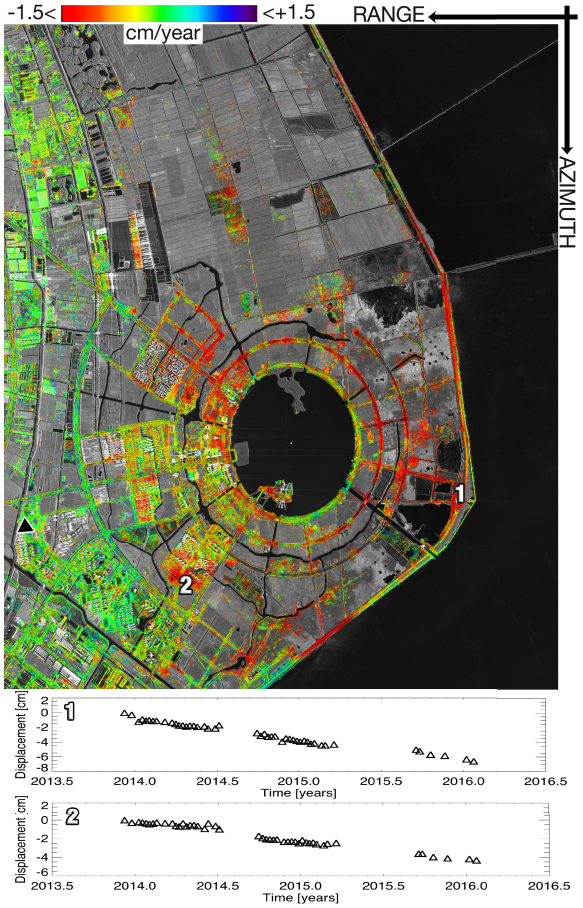

Fig. 3. InSAR products, focused on Lingang New City district, obtained from the proposed hybrid multiscale approach. The full resolution mean deformation velocity of the SL stable targets is present on the top, where are highlighted two PS targets of interest (labeled as 1–2). For the latter PS targets (1–2), the ground displacement time series are shown at bottom of the figure. The black triangle identifies the location of the spatial reference point.

grams. These phase residuals might affect the performance of the PhU operations at the SL scale that are usually carried out with conventional methods [12], [16], [17] by first fitting the phase residuals with a linear model and then inverting the relevant nonlinear phase components in the LS sense.

We show in Fig. 3 the mean ground displacement velocity map corresponding to well-processed SL pixels, characterized by temporal coherence values larger than 0.6. We also show the ground deformation time series of two selected PSs located in the area of land reclamation of the city of Shanghai. In Fig. 4, a comparison of the spatial distribution of the well-processed SAR pixels at the ML and SL scales [see Fig. 4(a) and (b)] is provided. It is also worth emphasizing that, with our method, the analysis of the SL interferograms does not require the preliminary generation of the ground displacement time series at the ML scale, with a consequent reduction of the overall processing computation time.

As a further experiment, we compared the number of well-processed SAR pixels obtained with our method with those obtained, using conventional methods [12], [16], [17], by fitting the (wrapped) phase residuals $\langle \varphi_m^{(\mathrm{SL})} - \psi_m'^{(\mathrm{ML})} \rangle_{-\pi,+\pi}$ with a linear model in time. With our method, well-processed SAR

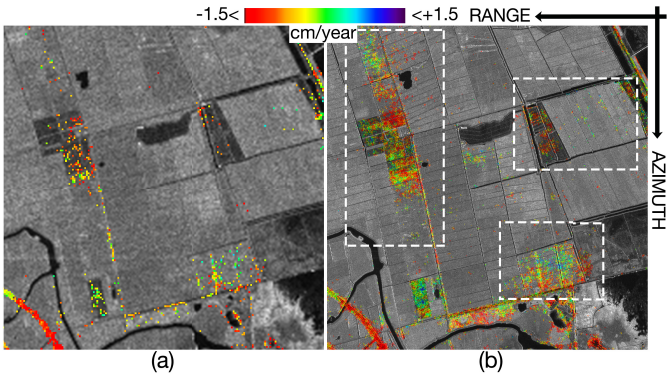

Fig. 4. Mean deformation velocity maps of a zoomed area of Lingang New City. (a) ML. (b) SL case. The white dashed rectangles highlight three regions of interest.

pixels at the SL scale were discriminated by computing the values of temporal coherence factor [10]. We obtained about 1.3 million pixels with temporal coherence values greater than 0.6. Conversely, in the conventional case, we used an alternative coherence factor [12], which quantifies the linear fitting accordance. In this case, we got about 650 000 pixels with coherence greater than 0.4. It is worth noting that the investigated land-reclaimed areas are subjected to significant

nonlinear ground deformations in time and this, along with the presence of spurious terms in the high-pass phase residuals, impacts the quality of the linear fitting. Moreover, we want also to point out that high temporal coherence values [10] denote that there is good agreement between the interferograms reconstructed from the generated ground displacement time series and the (wrapped) interferograms [18], thus providing a kind of indirect validation of the results.

V. Conclusion

A multiscale InSAR approach based on directly unwrapping the interferometric phases at the SL scale has been proposed. Unlike the multiscale InSAR approaches that use the information from the ML (regional) ground displacement time series to perform the full resolution PhU, in the proposed technique, exclusively, the ML unwrapped phases are employed. The strategy allows us to drastically reduce the amount of ambiguity numbers to be retrieved during the PhU operations at full resolution scale. Besides, with respect to alternative approaches, the method can straighforwardly process nonlinear/unmodeled deformation phase signals in time. This research study represents the first step. However, extra work is required to validate the method through ground-truth data in different applicative contexts characterized by heterogeneous ground deformation phenomena. This is a matter for future extensive investigations.

Acknowledgment

The authors would like to thank the Italian Space Agency (ASI) that provided the COSMO-SkyMed (CSK) SAR data in the framework of the European Space Agency-Ministry of Science and Technology of China (ESA-MOST) Dragon initiative (ID 10644 and ID 32294).

References

[1] R. Bamler and P. Hartl, "Synthetic aperture radar interferometry," *Inverse Problems*, vol. 14, no. 4, pp. R1–R54, Aug. 1998, doi: 10.1088/0266-5611/14/4/001.

[2] A. Ferretti, C. Prati, and F. Rocca, "Permanent scatterers in SAR interferometry," *IEEE Trans. Geosci. Remote Sens.*, vol. 39, no. 1, pp. 8–20, Jan. 2001, doi: 10.1109/36.898661.

[3] P. Berardino, G. Fornaro, R. Lanari, and E. Sansosti, "A new algorithm for surface deformation monitoring based on small baseline differential SAR interferograms," *IEEE Trans. Geosci. Remote Sens.*, vol. 40, no. 11, pp. 2375–2383, Nov. 2002, doi: 10.1109/TGRS.2002.803792.

[4] A. Hooper, "A multi-temporal InSAR method incorporating both persistent scatterer and small baseline approaches," *Geophys. Res. Lett.*, vol. 35, no. 16, pp. 1–5, 2008, doi: 10.1029/2008GL034654.

[5] J. Dong *et al.*, "Mapping landslide surface displacements with time series SAR interferometry by combining persistent and distributed scatterers: A case study of Jiaju landslide in Danba, China," *Remote Sens. Environ.*, vol. 205, pp. 180–198, Feb. 2018, doi: 10.1016/j.rse.2017.11.022.

[6] H. A. Zebker and J. Villasenor, "Decorrelation in interferometric radar echoes," *IEEE Trans. Geosci. Remote Sens.*, vol. 30, no. 5, pp. 950–959, Sep. 1992, doi: 10.1109/36.175330.

[7] D. C. Ghiglia and L. A. Romero, "Robust two-dimensional weighted and unweighted phase unwrapping that uses fast transforms and iterative methods," *J. Opt. Soc. Amer. A, Opt. Image Sci.*, vol. 11, no. 1, pp. 107–117, Jan. 1994, doi: 10.1364/JOSAA.11.000107.

[8] M. D. Pritt, "Phase unwrapping by means of multigrid techniques for interferometric SAR," *IEEE Trans. Geosci. Remote Sens.*, vol. 34, no. 3, pp. 728–738, May 1996, doi: 10.1109/36.499752.

[9] M. Costantini, "A novel phase unwrapping method based on network programming," *IEEE Trans. Geosci. Remote Sens.*, vol. 36, no. 3, pp. 813–821, May 1998, doi: 10.1109/36.673674.

[10] A. Pepe and R. Lanari, "On the extension of the minimum cost flow algorithm for phase unwrapping of multitemporal differential SAR interferograms," *IEEE Trans. Geosci. Remote Sens.*, vol. 44, no. 9, pp. 2374–2383, Sep. 2006, doi: 10.1109/TGRS.2006.873207.

[11] A. Pepe, L. D. Euillades, M. Manunta, and R. Lanari, "New advances of the extended minimum cost flow phase unwrapping algorithm for SBAS-DInSAR analysis at full spatial resolution," *IEEE Trans. Geosci. Remote Sens.*, vol. 49, no. 10, pp. 4062–4079, Oct. 2011, doi: 10.1109/TGRS.2011.2135371.

[12] R. Lanari, O. Mora, M. Manunta, J. J. Mallorqui, P. Berardino, and E. Sansosti, "A small-baseline approach for investigating deformations on full-resolution differential SAR interferograms," *IEEE Trans. Geosci. Remote Sens.*, vol. 42, no. 7, pp. 1377–1386, Jul. 2004, doi: 10.1109/TGRS.2004.828196.

[13] C. Ojha, M. Manunta, R. Lanari, and A. Pepe, "The constrained-network propagation (C-NetP) technique to improve SBAS-DInSAR deformation time series retrieval," *IEEE J. Sel. Topics Appl. Earth Observ. Remote Sens.*, vol. 8, no. 10, pp. 4910–4921, Oct. 2015, doi: 10.1109/JSTARS.2015.2482358.

[14] J. Ding *et al.*, "On the characterization and forecasting of ground displacements of ocean-reclaimed lands," *Remote Sens.*, vol. 12, no. 18, p. 2971, Sep. 2020, doi: 10.3390/rs12182971.

[15] M. Manunta *et al.*, "The parallel SBAS approach for sentinel-1 interferometric wide swath deformation time-series generation: Algorithm description and products quality assessment," *IEEE Trans. Geosci. Remote Sens.*, vol. 57, no. 9, pp. 6259–6281, Sep. 2019, doi: 10.1109/TGRS.2019.2904912.

[16] O. Mora, J. J. Mallorqui, and A. Broquetas, "Linear and nonlinear terrain deformation maps from a reduced set of interferometric SAR images," *IEEE Trans. Geosci. Remote Sens.*, vol. 41, no. 10, pp. 2243–2253, Oct. 2003, doi: 10.1109/TGRS.2003.814657.

[17] P. Blanco-Sánchez, J. J. Mallorquí, S. Duque, and D. Monells, "The coherent pixels technique (CPT): An advanced DInSAR technique for nonlinear deformation monitoring," *Pure Appl. Geophys.*, vol. 165, no. 6, pp. 1167–1193, Jun. 2008, doi: 10.1007/s00024-008-0352-6.

[18] A. Pepe, "Multi-temporal small baseline interferometric SAR algorithms: Error budget and theoretical performance," *Remote Sens.*, vol. 13, no. 4, Jan. 2021, Art. no. 4, doi: 10.3390/rs13040557.

[19] F. Falabella, C. Serio, G. Zeni, and A. Pepe, "On the use of weighted least-squares approaches for differential interferometric SAR analyses: The weighted adaptive variable-lEngth (WAVE) technique," *Sensors*, vol. 20, no. 4, p. 1103, Feb. 2020, doi: 10.3390/s20041103.